1 **Sensory convergence in the world's largest cavefish diversification: patterns of**

2 **neuromast evolution, distribution and associated behaviour in *Sinocyclocheilus***

3

4 Bing Chen[1], Tingru Mao[1], Yewei Liu[1], Wenzhang Dai[1], Xianglin Li[1], Jian Yang[2], Joshua

5 B. Gross[3], Madhava Meegaskumbura[1*]

6

7 [1] Guangxi Key Laboratory for Forest Ecology and Conservation, College of Forestry,

8 Guangxi University, Nanning, Guangxi, China

9 [2] Key Laboratory of Environment Change and Resource Use, Beibu Gulf, Nanning

10 Normal University, Nanning, Guangxi, China

11 [3] Department of Biological Sciences, University of Cincinnati, Cincinnati, OH 45221,

12 U.S.A.

13

14

15 Corresponding author *E–mail* : madhava_m@mac.com

16 **Abstract**

17 *Sinocyclocheilus* represents the largest freshwater cavefish genus in the world. This

18 emerging model system is endemic to the southern Chinese karstic landscape, and

19 demonstrates multiple adaptations for life in caves (troglomorphism), with eye-

20 degeneration being the most pronounced. The less-apparent lateral line system, which

21 is often expanded in cave-dwellers, has been studied in other cavefish systems, but

22 never in the context of this diversification. Here we investigated the distribution and

23 evolution of cephalic neuromasts in 26 *Sinocyclocheilus* species. We used live-staining

24 and behavioural assays, and interpreted results in a phylogenetic context. We show that

25 asymmetry in neuromast features and the rate of evolution is greater in cave-adapted

26 species. Ancestral state reconstructions show that most *Sinocyclocheilus* are right-

27 biased with some scatter, and show convergence of neuromast phenotypes. There is

28 substantial variation in cephalic neuromast distribution patterns between and (to a lesser

29 extent) within species. Behavioural assays show blind species have a distinctive wall-

30 following behaviour. We explain these patterns in the context of the deep evolutionary

31 history associated with this karstic region, other traits, and habitat occupation of these

32 remarkable diversifications of fishes. Interestingly, some of these neuromast patterns

33 and behaviour show convergence with other phylogenetically distant cavefish systems.

34

35 **Key words**: Asymmetry, convergence, ancestral state reconstructions, wall-following

36 behaviour, live staining, troglomorphisim

Background

Cave-dwelling (hypogean) fish provide a valuable system to study evolutionary novelty [1-4], owing to the extreme conditions associated with these habitats, such as limited food and perpetual darkness. Strong selective pressures arising from this extreme environment are associated with a suite of morphological changes, such as eye regression [5, 6]. However, numerous constructive features also evolve in cave-dwellers. Among the most notable are expansions of the mechanosensory lateral line system [7]. Here, we examine the nature of these expansions in the context of the species-rich genus *Sinocyclocheilus*, an emerging model system and the largest diversification of freshwater cavefish in the world [8, 9].

Neuromast organs are composed of hair cells with cilia embedded in a gelatinous cupula, surrounded by a complex set of support cells [10, 11]. There are two general neuromast types: canal neuromasts (CN), which are larger, and embedded in a bony canal, and superficial neuromasts (SN), which project directly from the skin epithelium [12-14]. In the Mexican tetra (*Astyanax*), cave morphs harbor variation in the number and size of both types of neuromasts, including several-fold more SNs compared to surface fish. Moreover, *Astyanax* cave morphs have a highly asymmetric distribution of neuromasts across left/right axis compared to surface morphs [15]. At present, it is unclear the relevance of this asymmetry, however, some studies suggest it may facilitate lateral swimming preference, rheotaxis (orientation towards flow), foraging, shoaling, predator avoidance, and mate-finding [7, 16-20].

Sinocyclocheilus are distributed across a vast 62,000 km^2 karstic area in Yunnan

59   and Guizhou Provinces and Guangxi Zhuang Autonomous Region [21, 22]. Based on

60   their habitat preference, these fish can be divided into three principal groups: troglobitic

61   (cave-restricted); troglophilic (cave-associated); and surface-dwelling [9]. It remains

62   unclear the extent to which the lateral line system has undergone changes associated

63   with these different habitats, however one study characterized neuromast size

64   differences between two *Sinocyclocheilus* species [20].

65   Here we examined numerical variation, lateral distribution and behavioural

66   differences associated with neuromasts in *Sinocyclocheilus*. Neuromasts may provide

67   functional compensation for eye loss, therefore we hypothesized that more severe

68   eye/vision loss may be associated with compensatory expansions of the lateral line

69   neuromasts. Specifically, troglomorphy was predicted to be associated with more, and

70   larger, neuromasts. Additionally, we anticipated a higher prevalence of distributional

71   asymmetry of neuromasts compared to surface fish, owing to relaxation of symmetry.

72   We found that neuromast distributions were asymmetric among all groups,

73   however the degree of asymmetry was most apparent for Regress-Eyed (collectively

74   both Blind and Micro-Eyed) species. Additionally, in phylogenetic contexts the pace of

75   neuromast evolution is faster among species with smaller eyes, compared to normal

76   eyed species. Taken together, this work provides the first diversification-wide

77   description of lateral line evolution, and clarifies the shared evolutionary pressure on

78   constructive trait evolution among distantly-related species that colonize caves.

79

80

4

81   **2. Methods**

82   *Sinocyclocheilus* adult fishes used in this study were examined using live, biosafe

83   staining techniques and behavioural assays. The project was approved by Guangxi

84   Autonomous Region Government and Guangxi University Ethical Clearance

85   Committee (# GXU-2021-125).

86   **(a) Fish maintenance in captivity**

87   Adult fish used in this study were collected from the field from 2017-2020 across

88   Yunnan and Guizhou Provinces and Guangxi Zhuang Autonomous Region of China

89   (figure 1, see geographic coordinates in electronic supplementary material: table S1,

90   figure S5). All fish were maintained in a centralized fish aquarium system, and

91   maintained at (pH: 7.0 - 8.0, temperature 19°C ± 1°C, dissolved oxygen 8.5mg/L).

92   Specimens larger than 5 cm were maintained in large glass aquaria (90 × 50 × 50 cm,

93   150 × 80 × 80 cm), with individual mechanical and bio-filters. For this study, 76

94   individuals from 26 *Sinocyclocheilus* species were used (table 1). *Carassius auratus* (n

95   = 3) and *Cyprinus carpio* (n = 3), two species from a closely related clade to

96   *Sinocyclocheilus* for comparison.

97

98

99

100

101

102

5

103   **Table 1.** Summary of 26 *Sinocyclocheilus* species used in the current analysis grouped

104   according to eyes morphology and habitat.

	Troglobitic (TB)	Troglophilic (TP)	Surface (S)
Blind (B)	*S. furcodorsalis* *S. tianlinensis* *S. tianeensis* *S. xunlensis*		
Micro-eyed (ME)	*S. mashanensis* *S. altishoulderus* *S. microphthalmus* *S. bicornutus* *S. rhinocerous* *S. cyphotergous*	*S. multipunctatus*	
Normal-eyed (NE)	*S. guilinensis* *S. huanjiangensis* *S. macrophthalmus* *S. guanyangensis* *S. brevis* *S. lingyunensis* *S. zhenfengensis* *S. jii* *S. yishanensis*	*S. longibarbatus*	*S. angustiporus* *S. oxycephalus* *S. malacopterus* *S. purpureus* *S. maitianheensis*
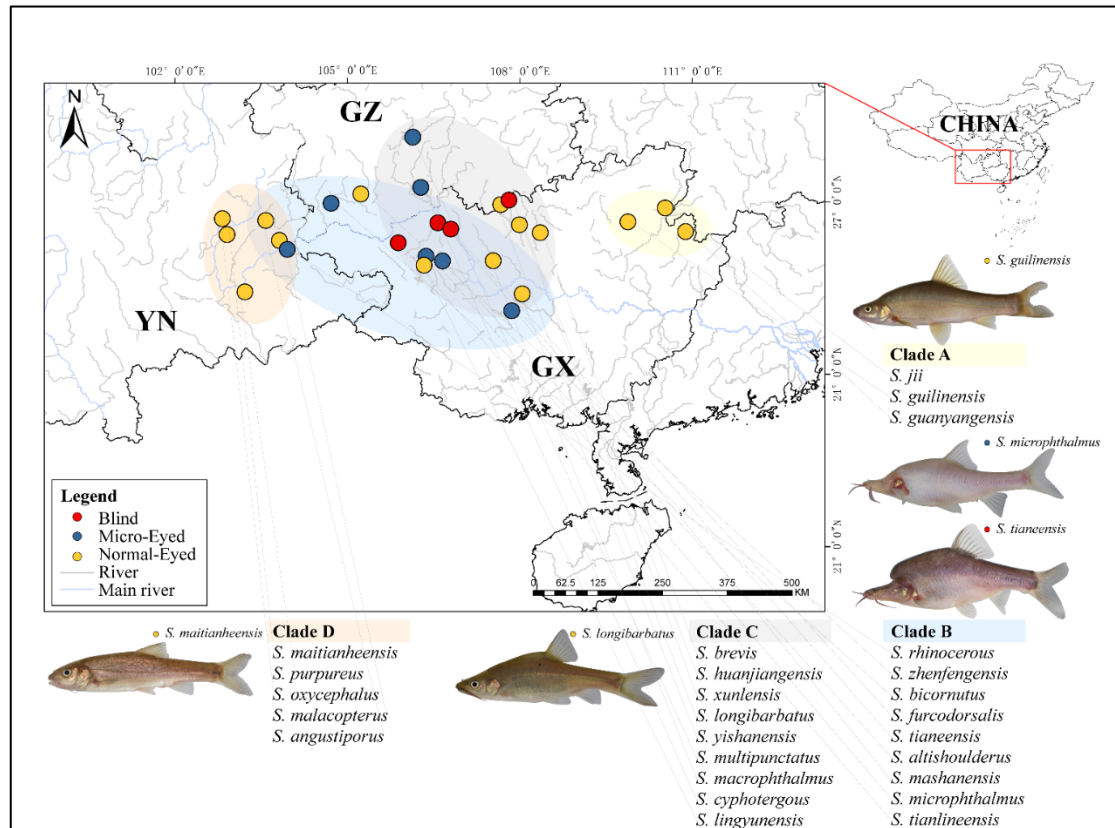
Figure 1. Map showing the distribution of sampling sites of the 26 species of *Sinocyclocheilus* (n = 76) used in this study. These fishes are mainly distributed across South China's Karstic habitats on three provinces: Guangxi Autonomous region (GX), Guizhou (GZ) and Yunnan (YN). The four main clades (A – D, represented by a color code), the species used from each clade, and a representative photo of species from these clades are shown. Early emerging Clade A is mainly distributed in the eastern range of the diversification and Clade D to the hills to the West; Clade B and C contain the most troglomorhpic species and are distributed mainly across GX and GZ. The eye-condition (Blind, Micro-eyed and Normal-eyed) are depicted using a color code.

(b) Vital staining of neuromasts

To visualize bones and neuromasts, live fish were immersed in 1mg/L Calcein-AM

7

118 (C0875-5G; Sigma-Aldrich) and 20μg/ml DASPEI (D0815; Sigma-Aldrich) [15, 23,

119 24]. Fish were anesthetized using MS222 (E808894-5g; Macklin) 0.01-0.02g/L for 3-6

120 min followed by brief immersion in ice water for ~20s, depending on size and age (e.g.,

121 smaller specimens were exposed to ice water for shorter periods). All individuals were

122 continuously monitored to ensure the health and safety of experimental individuals.

123 **(c) Digital Analysis of Neuromasts Position and between Distances**

124 This study focused on the cephalic region anterior to the opercular and interopercular

125 bones, near the arc on the lateral aspect [20, 22]. Images were collected using a Leica

126 M165FC fluorescent stereomicroscope outfitted with Leica Application Imaging

127 software (LAS X v3.4.2.18368). The dorsal, left and right aspects of each individual

128 were imaged under identical conditions. High-definition "montage" image were

129 consolidated following automated alignment and 'flattening' of 30 images collected in

130 the z-plane (× 9/ 13/ 16 magnification) using LASX or Helicon Focus (Pro v7.6.1), to

131 perform the two-dimensional shape images. The use of montage imaging minimized

132 potentially confounding variables arising from the z-plane for each specimen.

133   The outline of fish and neuromast positions were obtained using the "Pencil" and

134 "Point" tool in GIMP (v2.10.24). Neuromast numbers were quantified using an

135 automated method in ImageJ (v1.8.0), following the method of Gross et al. (2016) [15].

136 For ambiguous images, we performed direct, manual counting (figure 3*a*). We

137 calculated the size (2-D area) of individual neuromasts, lens, and eye orbit diameter by

138 determining their size in pixels using the "measure" function in ImageJ and converting

139 to mm^2. We also used a vernier caliper to measure standard length (SL). To determine

8

140   the density of neuromast within particular unit areas, we used "Delaunay Voronoi"

141   triangulation in ImageJ to define a proxy for the mean distance between neuromasts

142   [25-27] (figure 3*a*).

143   **(d) Quantifying symmetry**

144   To examine positional symmetry of neuromasts across the left-right axis, we

145   manually superimposed the fluorescent images of neuromasts (figure 3*b*). We used

146   excitation filters for three colors (Blue 470/40 nm, Texas Red 560/40 nm and Green

147   546/10 nm). In GIMP, we then reflected the left images to align with the right images,

148   creating a single image. We measured the scoring of neuromasts in the reverse sequence

149   (right-side first) relative to the initial scoring of neuromasts (left-side first) to avoid bias

150   in our calculations [28].

151   The "colocalization" [29, 30], and "JACop" [31, 32] plugins in FIJI were used to

152   calculate an asymmetry coefficient [15, 33, 34]. We performed a Pearson's correlation

153   to compare the intensity distribution between channels [35]. Next, we calculated an

154   Overlap Coefficient (OC), to identify positional overlap of signals from the left and

155   right sides [36]. This enabled us to quantify the extent to which positions of neuromasts

156   on the left and right sides of the cranium were symmetric (figure 3*a*).

157   We divided 26 species into Regressed-Eyed groups (containing Blind n = 12, and

158   Micro-Eyed n = 21) and Normal-Eyed groups (n = 45), following the categorization

159   and phylogeny of Mao et al. (2021). Importantly, a few *Sinocyclocheilus* species do not

160   have uniform eye sizes [22]. For instance, *S. guanyangensis* have highly variable eye

161   sizes, so for this study we selected individuals with the most normal eye morphology.

9

162   All parametric neuromast measures were subjected to one-way ANOVA with a post-

163   hoc Tukey test analysis. Non-parametric distributions were subjected to Wilcoxon

164   Signed Rank Test (2-tailed, Holm correction) or a Kruskal-Wallis test with a post-hoc

165   analysis Dunnett test (2-tailed, Bonferroni correction). Statistical significance was set

166   at $p < 0.05$. We used the packages "wmc" and "FSA" in R (v3.6.3). Principal

167   Component Analysis (PCA) was used to evaluate the following variables: number, area,

168   asymmetry coefficients and mean distance. To analyse the relationships between

169   Regressed-Eyed and Normal-Eyed groups, we performed Spearman's rank correlation

170   coefficients using SL, eye traits, area, number, mean distance and OC of neuromasts

171   patterns.

172   **(e) Phylogenetic inference**

173   To study the patterns of neuromast evolution in *Sinocyclocheilus,* we inferred a

174   phylogenetic tree for the 26 species, using two available gene fragments from Genbank

175   (NADH-ubiquinone oxidoreductase chain 4 - ND4 and cytochrome b gene – Cyt b),

176   together with an outgroup species (*Cyprinus carpio*) (table S1). We used two different

177   methods for phylogenetic inference [37] – Bayesian and Maximum Likelihood for tree

178   construction (alignment, model selection and phylogenetic inference method details are

179   available in the electronic supplementary material, Supplementary Methods).

180   **(f) Evolution rate analysis**

181   To test the allometric evolution rate between neuromasts in different morphs [9],

182   we analysed neuromast numbers, left/right-side numbers, mean distance coefficient,

183   area and density (i.e. the proportion of number and area anterior to the gill). We used

184   100 potential trait histories from stochastic character mapping, and fit two alternative

185   models (single or multiple rate model, calculated by AIC) of evolution for each studied

186   trait. In the case of small samples, we assumed the AIC and AICc to assess, and then

187   weighted from Bayesian analyses on the trees using the brownie.lite function. We used

188   the package "rgl", "ape" and "phytools" in R to calculate the model-averaged estimates

189   [38].

190   **(g) Patterns of neuromasts evolution using ancestral state reconstructions**

191   To understand the broad patterns of neuromast evolution in *Sinocyclocheilus*, we

192   classified 26 species into the following three morphological groups: (1) Left-right axis

193   asymmetry: according to different degree of overlapping coefficient, divided as

194   Absolute-asymmetry (OC < 0.1) and Slight-asymmetry (OC ≥ 0.1) based on Gross et

195   al. (2016) [15]. (2) Left/right-bias handedness: we used the normalized SN number by

196   signed (directional) asymmetry rate: $SAR = \frac{R-L}{R+L} \times 100\%$ following Planidin et al. (2021)

197   [39], which suggests the presence of two morphological categories: Right-biased (SAR

198   > 0, neuromasts on right-side mainly) and Left-biased (SAR < 0, figure S1). (3)

199   Distance expansion: depending on the results of neuromasts mean distance coefficient,

200   we divided species into Scattered (DEL > 0.2) and Serried (DEL ≤ 0.2), following

201   Gross et al. (2016) [15] (table S1) .

202   To understand the evolution of neuromast patterns, we performed ancestral state

203   reconstructions using these three morphological categories. One hundred stochastic

204   reconstructions were simulated through the stochastic mapping approach that was

205   conducted using function "make.simmap" (model = "ER") in the R packages "ape",

11

206 "phytools" and "viridisLite".

(h) Cave-dwelling behaviour associated with neuromast variation

208 To understand how neuromast patterns may facilitate certain behaviour, we carried out

209 a series of behavioural assays. All assays were performed using the following 14 species

210 (n = 3 individuals for each): Blind - *S. furcodorsalis, S. tianlinensis, S. tianeensis*;

211 Micro-Eyed - *S. mashanensis, S. microphthalmus, S. bicornutus, S. multipunctatus*;

212 Normal-Eyed - *S. guilinensis, S. longibarbatus, S. macrophthalmus, S. oxycephalus, S.*

213 *zhenfengensis, S. purpureus, S. maitianheensis*. Each experimental fish was

214 acclimatized for 30 min in a rectangle assay arena (45 × 28 × 28 cm) in system water.

215 An infrared camera (Cannon XF400/405) was used to capture video under infrared light

216 in a quiet, dimly lit room (frame rate: 4Mbps (VBR, YCC 4:2:0, 25p, 1280 × 720).

217   Wall-following behaviour has been observed in *A. mexicanus* cavefishes; therefore,

218 we examined a range of wall-following within the arena. This included fish swimming

219 a minimum distance of its SL along the wall, or a distance of ≤ 0.5 SLs away from the

220 wall (figure 5*a-b*) [40, 41]. We recorded normal tracking without stimulation for 10-

221 min to determine if wall-following behaviour was present using EthoVision XT (v15.0 ,

222 Noldus) alongside direct visual monitoring. (2) We next used an aeration pump (45~50

223 Hz vibration) for 5-min to record the approaching of a novel object in modified

224 vibration attraction behaviour test [42-44]. We selected the area centered on the

225 stimulation model based on tank shape (10 × 16 cm). We monitored the frequency of

226 time spent in the stimulation range from left/right-side. Data analysis were performed

227 in R's basic functions as mentioned.

228

Results and Discussion

All cavefish species, for which neuromast distribution has been studied, are asymmetric [15, 45-48]. Accordingly, we found the two outgroup species of Cyprinidae did not show a comparable pattern of neuromast asymmetry as was observed in *Sinocyclocheilus*. Fish living in perpetual darkness frequently lose vision while enhancing non-visual sensation, such as the lateral line [42, 49, 50]. Here we show that *Sinocyclocheilus* similarly conform to this pattern (figure 2). Additionally, widespread neuromast distributional asymmetry in *Sinocyclocheilus* is convergent with other distantly related cavefish species inhabiting similar cave microenvironments. Interestingly, our results showed that this asymmetric neuromast pattern is variable across the 26 *Sinocyclocheilus* species tested, with most species demonstrating a right-sided bias (figure 4). Evidence for neuromast asymmetry patterns in other lineages comes from two lineages from Central and North America: *Astyanax mexicanus,* with a left-side bias and the *Gasterosteus aculeatus* (stickleback fish), with a right-side bias [39, 51]. These results reveal variation in "sidedness" across taxa, despite convergence in asymmetry.

(a) Patterns of neuromast symmetry and asymmetry

The neuromasts distribution pattern showed asymmetry across the left-right axis, with variation both within and across species (figure 2*a*, table S2). Interestingly, mean overlap coefficients indicated that all species showed a degree of neuromast asymmetry. Normal-Eyed species showed the least asymmetry, while Blind species showed the

250 highest and Micro-eyed species had intermediate values (mean ± s.d.: Normal-Eyed =

251 0.098 ± 0.05; Blind = 0.091 ± 0.031; Micro-eyed = 0.096 ± 0.027; $H_2 = 0.64$, $p > 0.05$).

252 This finding is consistent with prior work suggesting that asymmetry may facilitate

253 navigation in darkness [52, 53], foraging [54] and the ability to maximize sensory

254 information using fewer receptors [39, 51]. In comparing asymmetry measures across

255 clades, Clade D (all Normal-Eyed living in surface, showed as: N-S; mean ± s.d. =

256 0.119 ± 0.058) showed the least asymmetry, while Clade C (mean ± s.d. = 0.079 ± 0.031)

257 showed the highest asymmetry; with Clade A and B demonstrating intermediate values

258 (Clade A – 0.086 ± 0.029 and Clade B – 0.104 ± 0.038).

259

260
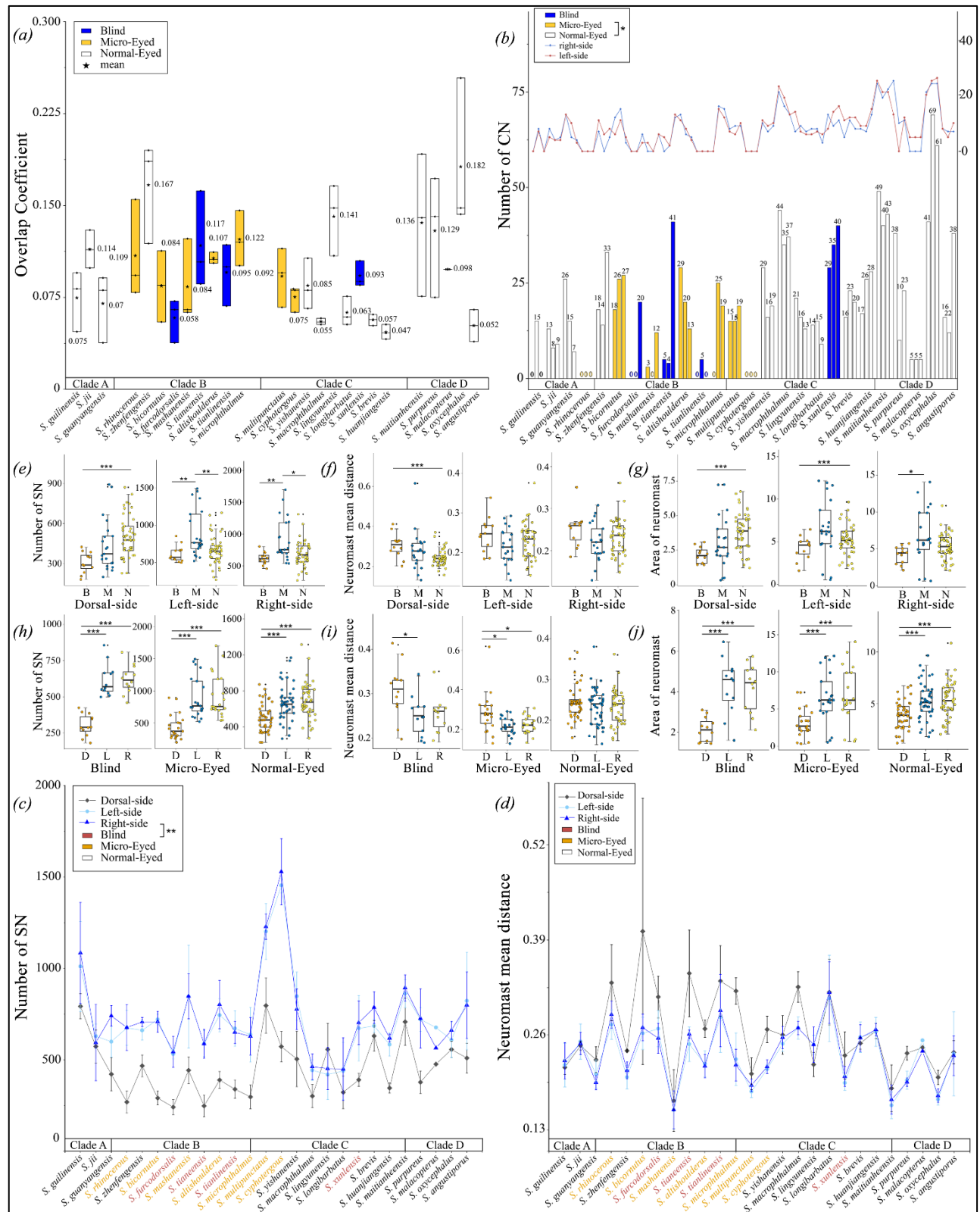
Figure 2. Comparison of neuromast-related measurements for 26 species of

Sinocyclocheilus **(n = 76).**

(a) The average scores of Overlapping Coefficient (OC) measured as the pattern of

264   neuromasts on left/right-side of the fish. The standard of asymmetry results is defined

265   as: asymmetry (OC < 0.1), symmetry (OC ≥ 0.1). Clade A-D represent the clade level

266   relationships of these 26 species in the phylogenetic tree. All statistical results are

267   available in table S1, S2.

268   (b) The bars represent the individual's canal neuromasts (CN) total counts and the lines

269   represent the left and right sides of cephalic CN in different species. The CN of Micro-

270   Eyed species was significantly less than Normal-Eyed species (H = -2.64, p = 0.025).

271   (c) The mean number of superficial neuromasts (SN) on the cephalic area (dorsal, left

272   and right sides) in different *Sinocyclocheilus* species.

273   (d) The mean surface area covered by SN on the dorsal/left/right-side of different

274   *Sinocyclocheilus* species. The surface species covered by the dorsal SN are less than

275   that of the surface are covered by the right and left sides of fish.

276   (e-g). The comparisons about: (e) the number of SN; (f) neuromasts mean distance

277   coefficient; (g) area of SN on Dorsal/Left/Right-side on cephalic area. Group divided

278   by the Blind (B in orange), Micro-Eyed (M in blue) and Normal-Eyed (N in yellow).

279   The Wilcoxon signed rank (2-tailed, Holm correction) test suggested that the surface

280   covered by dorsal neuromasts are significantly less than that covered by the right and

281   left sides. *: P < 0.05, **: P < 0.01, and ***: P < 0.001. All statistical results are

282   available in table S2, S5.

283   (h-j). The comparisons of the non-parametric statistical tests performed for (h), the

284   mean number of SN; (i) neuromasts mean distance coefficient; (j) mean area of SN on

285   the cephalic area of the Blind, Micro-Eyed and Normal-Eyed morphs. The comparisons

286   were sub-divided into dorsal-side (D in orange), left-side (L in blue) and right-side (R

287   in yellow) for visualization purposes.

288

289   **(b) Patterns of neuromast distribution**

290   Generally, we found more SNs on the right compared to the left-side, however we

291   observed substantial variation between and across species. We examined distributions

292   in three aspects: dorsal, left and right sides. In the dorsal aspect, Blind fish have the

293   least, Normal-Eyed fish have the most, and the Micro-Eyed group was intermediate

294   (figure 2*e*). Unexpectedly, there were significantly fewer SNs in Blind species (mean ±

295   s.d.: Blind = 1543 ± 248; Micro-Eyed = 2252 ± 802; Normal-Eyed = 1859 ± 504; H_2 =

296   10, p = 0.0065, table S5). In terms of lateral distribution, Blind and Normal eyed fish

297   had higher numbers on the right-side, while Micro-Eyed species had more neuromasts

298   on the left-side (median: left = 767, right = 758; W = 227, p = 0.890; figure 2*h*; table

299   S5).

300   We found that dorsal neuromast numbers are significantly lower than the lateral

301   sides. An interesting exception was *S. lingyunensis* (N-TB, Clade C), dorsally

302   distributed neuromasts outnumbered laterally-situated neuromasts (mean dorsal = 557,

303   left = 419, right = 453; figure 2*c*, table S5). In the dorsal aspect, Normal-Eyed species

304   had the most neuromasts, while the Blind group had the fewest. One potential

305   explanation for this difference could be that obligate subterranean fishes experience

306   relaxed selective pressure (e.g. aerial predation from birds) [21, 55], but perhaps dorsal

307   neuromasts are necessary for navigation within caves [56].

308   With respect to neuromast expansion (scatter), we found that the most scattered

309   SNs are dorsal, especially in Blind species (mean ± s.d.: Blind = 0.31 ± 0.06; Micro-

310   Eyed = 0.28 ± 0.10; Normal-Eyed = 0.24 ± 0.04; H_2 = 12, p = 0.002; figure 2*f*, table

311   S5). Additionally, neuromasts tend to be more scattered on right- compared to the left-

312   side across all three groups (median right/left Blind = 0.26, 0.25; Micro-Eyed = 0.22,

313   0.21; Normal-Eyed = 0.24, 0.23; figure 2*d*). Interestingly, the Blind cavefish group

314   demonstrated the most scatter, while the Micro-Eyed group had the least scatter (figure

315   2*i*, table S5). In Mexican cavefish, *Astyanax* demonstrates more scatter in the surface

316   forms compared to *Sinocyclocheilus* [15, 57], however this is likely due to the fact that

317   *Astyanax* Blind forms have more neuromasts, and hence less scatter.

318   In the comparison of surface area covered by neuromasts, we found a significantly

319   lower surface area populated by neuromast dorsally, with the Blind group having the

320   smallest area (mean ± s.d. Blind = 2.14 ± 0.59; Micro-Eyed = 3.13 ± 1.94; Normal-

321   Eyed = 3.88 ± 1.33; H_2 = 15.9, p = 0.0003; figure 2*j*). When comparing lateral sides,

322   we found the total distributional area of neuromasts to be highly comparable within

323   groups (median right/left-side Blind = 4.44, 4.6; Micro-Eyed = 6.19, 6.21; Normal-

324   Eyed = 5.31, 5.14; table S5). Normal-Eyed species have the largest area of neuromast

325   distribution, Micro-Eyed fish have an intermediate area, and the Blind group had the

326   smallest area covered by (mean ± s.d. = 10.56 ± 2.95; Micro-Eyed = 16.44 ± 8.80;

327   Normal-Eyed = 14.49 ± 4.59; F = 3.83, p=0.026; figure 2*g*). Although it has been shown

328   that the neuromast complexity of the Blind species is greater than Normal-Eyed species,

329   this however, has not been established at a diversification-wide scale.

18

330   Blind *Sinocyclocheilus* have fewer CNs compared to Normal-Eyed

331   *Sinocyclocheilus* (median Blind = 5, Micro-Eyed = 13; Normal-Eyed = 17; table S5),

332   reflecting the same pattern as SNs. For *Astyanax*, surface fish are invariant in terms of

333   numbers, but cavefish are highly variable. Surprisingly, two species, *S. rhinocerous*

334   and *S. cyphotergou* appeared to possess no CNs (both M-TB, figure 2*b*), suggesting

335   the canal lateral line system may have regressed in this species. Interestingly, a similar

336   phenomenon has been observed in Amblyopsid cavefish (Teleostei: Percopsiformes)

337   [47] and in Threespine Sticklebacks (*Gasterosteus aculeatus*) [58].

338   In sum, neuromasts are generally reduced in number and area in Blind species, but

339   not in scatter (expansion). Somewhat surprisingly, Micro-Eyed species had the most

340   neuromasts, greater area, and least dense distribution of neuromasts. We propose that

341   Blind species may have optimized adaptation to the subterranean biome by using fewer,

342   but more complex, neuromasts. Blind *S. tianlinensis*, for instance, have SNs with

343   greater diameters and more hair cells compared to Normal-eyed *S. macrophthalmus*

344   [20].

345   **(c) Correlations between asymmetry and eye condition**

346   We performed a Spearman Rank's correlation of the highly loading variables for

347   the Regressed-Eyed and Normal-Eyed. In the Regressed-Eyed group, eye measures

348   demonstrated a significantly positive correlation with neuromasts number ($\rho = 0.7$, p <

349   0.001) and area ($\rho = 0.7$, p < 0.001) , but a slightly negative correlation with mean

350   distance between neuromasts ($\rho = -0.3$, p < 0.05). In the Normal-Eyed group, eye

351   measures had a significantly positive correlation with neuromasts area ($\rho = 0.4$, p <

352 0.005) and mean distance (ρ= 0.4, p < 0.05) , but significantly negative correlation with

353 the results of asymmetry (ρ= -0.4, p < 0.001; figure 3*d,e*, table S4). Overall, the

354 Regressed-Eyed group is more asymmetric compared to Normal-Eyed group.

355
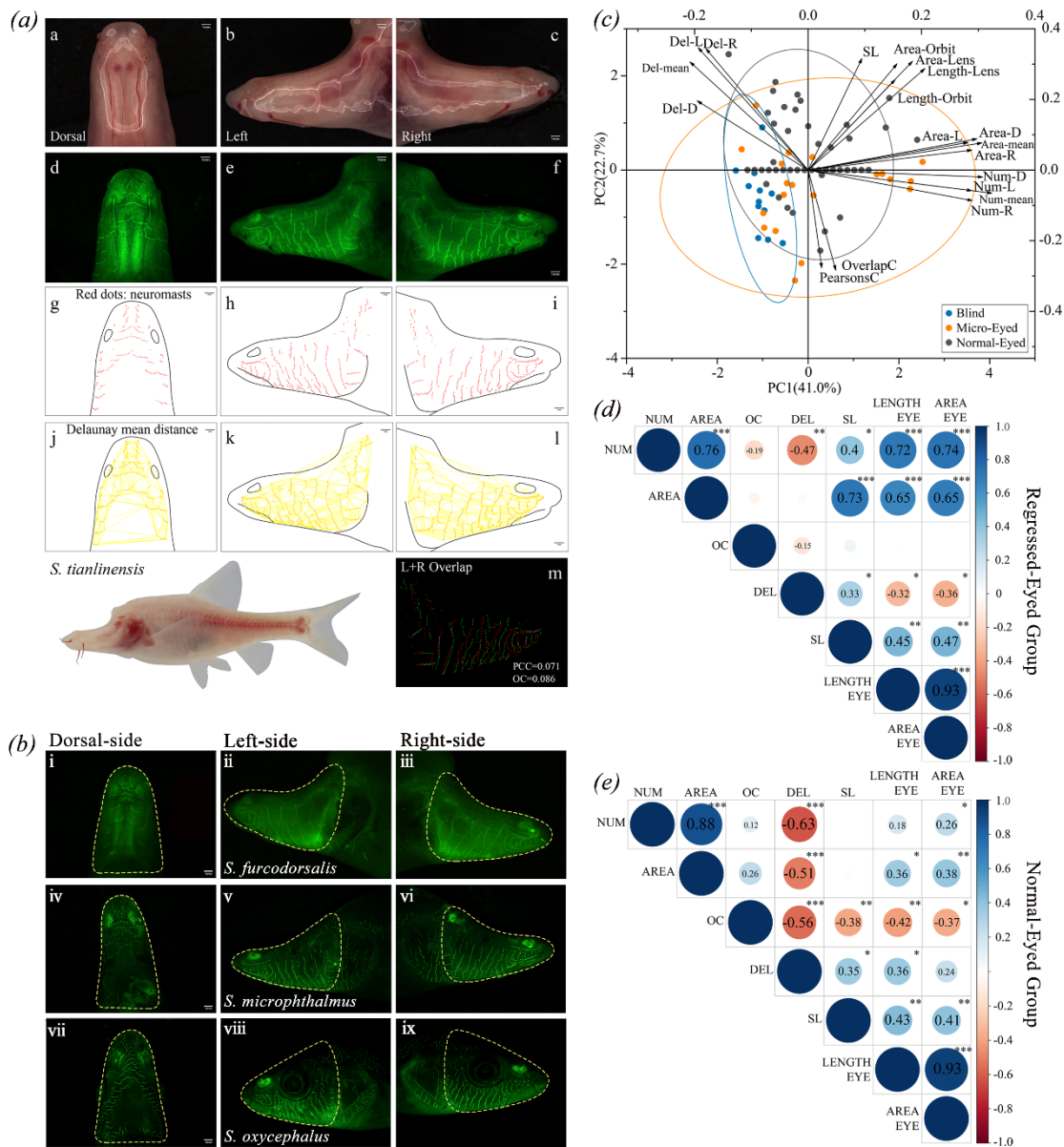
Figure 3. Summary of fluorescent staining results for different cavefish morphs.

357 (a) the fluorescent staining results of *S. tianlinensis* (Blind species-Troglobitic, B-TB).

358 (table 1 & table S1).

359 (a-c) photos taken under normal lights. (d-f) dorsal, left and right sides of the

20

360   neuromasts under fluorescent light. (small green dots are SN, bigger green dots are CN).

361   (g-i) The diagrammatic representations of the dorsal, right and left side neuromasts.

362   SNs denoted by red dots and the area outlined in black represent cephalic region and

363   the olfactory area. (j-l) The neuromasts mean distance measures as the "Delaunay Mean

364   Distance" are indicated by yellow lines. (m) The asymmetry values calculated by

365   overlap coefficient. Red and green dots represent the left and right sides of the fish.

366   Note that the scale of the images is the same at the length of 1.0 mm.

367   (b) The results of the fluorescent staining of three cavefishes, (i-iii) *S. furcodorsalis,*

368   (iv-vi) *S. microphthalmus* and (vii-ix) *S. oxycephalus,* used as representatives of each

369   eye-related morphs. These three species are classified as (B-TB), Absolute-

370   asymmetry/Scattered/Left-bias; (M-TB), Slight-asymmetry/ Scattered/Right-bias and

371   (N-S), Slight-asymmetry/Serried/Right-bias respectively. Scales of the images are the

372   same at the length of 1.0 mm.

373   (c) Principal Component Analysis (PCA) bi-plot for the distribution traits of neuromasts

374   in *Sinocyclocheilus*.

375   The dorsal/left/right-side and mean counts number (Num-D, Num-L, Num-R, NUM);

376   dorsal/left/right-side and mean distance coefficient (Del-D, Del-L, Del-R, DEL);

377   asymmetry coefficients of neuromasts (PearsonsC, OverlapC); eyes traits (area of

378   lens/orbit (Area-Lens, Area-Orbit) and length of lens/orbit (Length-Lens, Length-

379   Orbit)) with standard length [5] were included as variables in the PCA. All results are

380   available in Supplemental table S2, S3.

381   (d) The Correlations between SN number (NUM), area (AREA), mean distances

382   coefficient (DEL) and asymmetry coefficient (OC) of neuromasts; standard length [5]

383   and the length of lens (LENGTHEYE) and area of lens (AREAEYE). The   scores

384   indicate the results of the spearman's rank correlation coefficient $|\rho|$; $< 0.3 =$ no

385   correlation, $0.3\text{-}0.8 =$ low correlation, $> 0.8 =$ high correlation. Positive correlations ($\rho >$

386   0) and negative correlations ($\rho \leq 0$) are shown in blue and red colors respectively. *: P

387   < 0.05, **: $P < 0.01$, and ***: $P < 0.001$ indicate the level of statistical significance. All

388   results are available in table S4.

389

390   **(d) Dimensionality of the neuromast variables**

391   We performed a principal component analysis (PCA) based on 26 species of

392   *Sinocyclocheilus* and their neuromast-related variables, to identify key features

393   underlying neuromast variation. PC1 was explained mostly by the number of

394   neuromasts (mean number: NUM, counts on dorsal side: Num-D) and the total

395   neuromast distributional area (AREA). PC2 was explained mostly by the distances

396   between neuromasts (mean distance coefficient on left side: Del-L, on right side: Del-

397   R; table S3). The 95% confidence intervals for each group shows that intraspecific

398   variation in Blind group were the narrowest, while the Micro-Eyed group showed the

399   highest variation (figure 3*c*). This may be explained by the fact that Micro-Eyed forms

400   are subjected to selective pressures of both surface habitats, subterranean habitats and

401   the transitional habitats between these [22, 59, 60]; i.e. habitat heterogeneity.

402

403   **(e) Patterns of neuromasts evolution**

404   We next performed an ancestral reconstruction for three character states: asymmetry,

405   handedness and neuromasts expansion. We found the deeper nodes in the phylogeny

406   showed ambiguity for asymmetry and handedness (see maximum credibility tree;

407   figure 4). However, the deeper nodes for neuromast distribution suggested a scattered

408   distribution of neuromasts is the ancestral condition. In *Sinocyclocheilus, ~* 70% of

409   the species examined demonstrate right-handedness. Our ancestral state

410   reconstruction shows an entire clade of 7 species is right-handed. However, both left-

411   and right-handed mixed clades and sister taxa are present within the diversification,

412   suggesting this is a variable trait. In contrast, ancestral state reconstructions show

413   nearly 80% of the *Sinocyclocheilus* have scattered neuromast distributions.

414   Additionally, all Blind species showed a scattered neuromast pattern of distribution.

415   (figure 4*c*; black arrow).
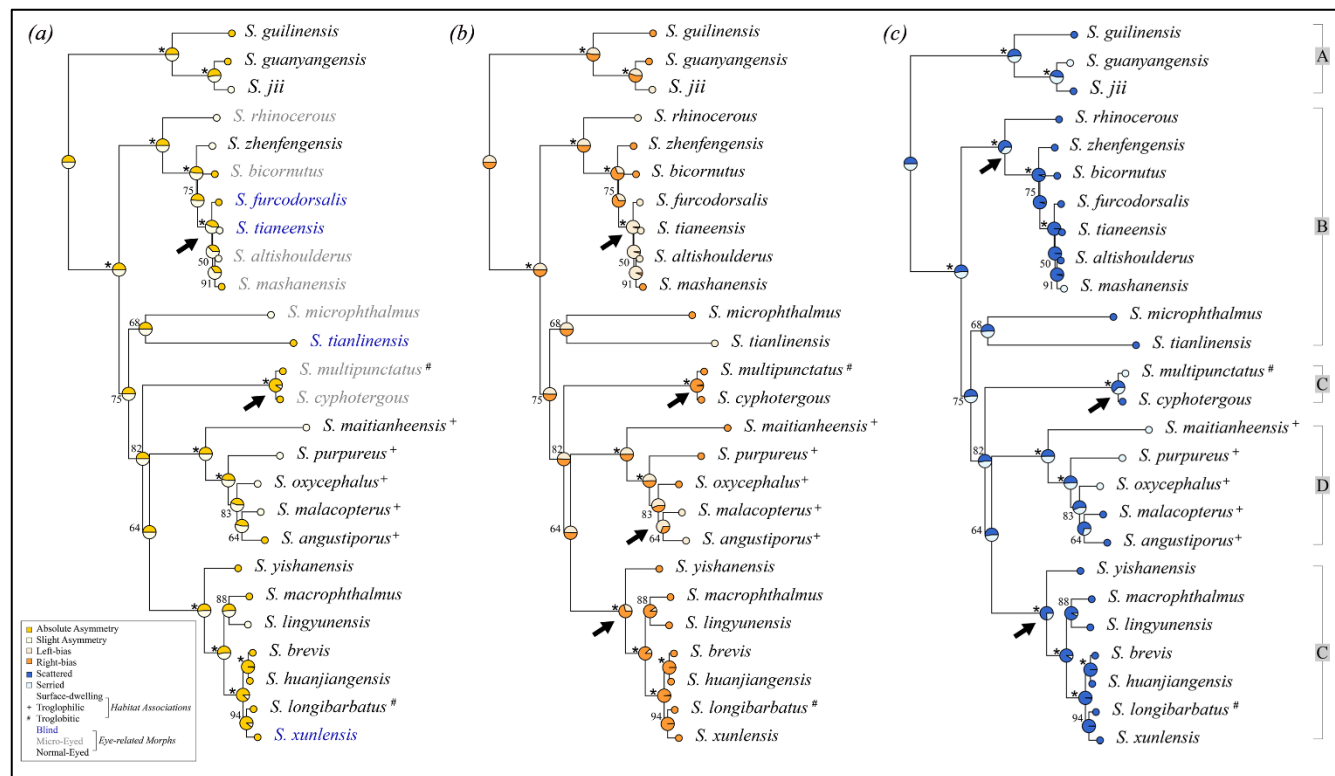
416

417   **Figure 4. Patterns of cephalic neuromast trait evolution of *Sinocyclocheilus* based**

418 **on ancestral state reconstruction on the maximum-likelihood tree.** Ancestral state

419 reconstructions based on the Bayesian inference method is shown in figure S2-S4.

420 (a) Ancestral state reconstruction using stochastic character mapping for symmetry in

421 neuromasts pattern (Absolute/Slight-asymmetry). The tip colors represent state of the

422 extant species and each node indicates the ancestral state as a proportion of the tip state.

423 A, B, C and D showed on the extreme right of the figure indicate four major clades.

424 The bootstrap values > 95% are indicated as * on nodes.

425 (b) Ancestral state reconstruction using stochastic character mapping for handedness

426 bias (Left/Right-bias) on the phylogeny.

427 (c) Ancestral state reconstruction using stochastic character mapping for neuromast

428 expansion (Scattered/Serried) on the phylogeny.

429

430 **(f) Evolution rates analysis**

431 Among cavefish, the rate of neuromast evolution has only been determined for

432 *Sinocyclocheilus.* The rate of scatter for Blind species is higher compared to others

433 (mean distance and density - 3.5 and 6.8 times increased than Normal-Eyed species),

434 and the rate of numerical expansion of neuromasts is 1.2 times greater in Micro-Eyed

435 species (table 3). Normal-Eyed *Sinocyclocheilus* species demonstrated lower

436 evolutionary rates for every character state. A multiple-rate model of evolution

437 provided the best fit for mean distance between neuromasts, relative neuromast

438 density and neuromast distribution area. However, a single-rate model of evolution

439 provided the best fit for traits associated with neuromast numbers (table S6). Thus, the

24

440   evolutionary rate of cave-related neuromast patterns were highest in cave adapted

441   forms. Further, rates of evolution for surface area covered by SN neuromasts, and

442   right-sided neuromast numbers, are moderately increased in Blind and Micro-Eyed

443   species.

444   **Table 2.** Model-averaged rate parameters for the measured traits of neuromasts in

445   eyes-related morphs of *Sinocyclocheilus* species. **Bold font** = highest rate

446

Trait	Average rate		
	Blind	Micro-Eyed	Normal-Eyed
Number	155.1042	**179.4815**	150.6202
Left Number	**0.6395**	0.4106	0.4249
Right Number	**0.7095**	0.5056	0.5329
Area	102.8836	**106.2819**	101.9520
Mean distance	**34.4129**	11.7357	7.9001
Density	**362.2959**	64.3977	42.2944

447   **(g) Behavioural correlates of neuromasts**

448   We performed a series of behavioural assays, and found that Blind species

449   navigate markedly differently from eyed-species. Blind species have a well-

450   established wall-following behaviour, while sighted species utilize an entire arena

451   space (figure 5). We found that Blind species prefer to use the side with fewer

452   neuromasts for wall-following, but the side with more neuromasts for exploring (i.e.,

453   stimulation during VAB test). Micro-Eyed species having a left-bias in neuromast

454   distribution, and approached a stimulation area from the left-side (median = 4) more

455   frequently than right-side (median = 3; W = 612, p > 0.05). These species, however,

456   followed the wall on their right-side (median = 154) for a significantly longer time

457   compared to the left-side (median = 142; W = 967, p < 0.001; figure 5*c,g*; table S5).

25

458   Behavioural heatmaps depicting wall-following behaviour showed that Blind species

459   prefer swimming in a fixed route, but eyed-species swam in irregular patterns (figure

460   5 *d-f'*).

461   Wall following behaviour has also been characterized in *Astyanax mexicanus*. In

462   this species, blind morphs similarly use the side with fewer neuromasts towards the

463   wall, perhaps to use the contralateral side for detecting stimuli important for feeding,

464   communication and spatial learning [17, 42]. This divergence occurred during the

465   geological uplift of the Yunnan-Kweichow Plateau together with the aridification of

466   China, which occurred during the Pliocene and the Pleistocene [61]
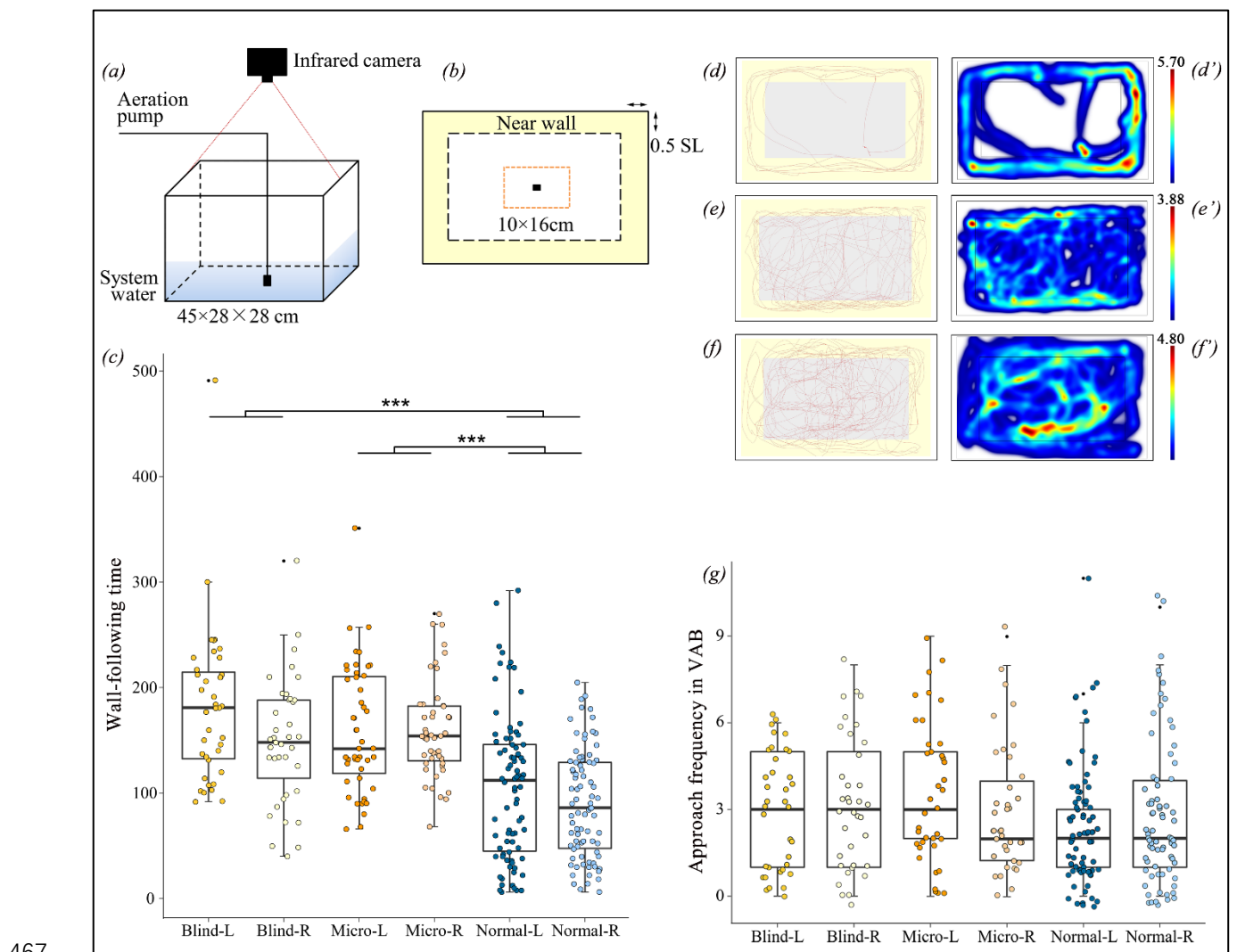
467

468 **Figure 5. The experimental setup and results of the behavioural assays.**

469 (a) Schematic diagram showing the assay system used to for the wall-following and

470 vibration attraction behaviour (VAB).

471 (b) The vertical view of the arena's schematic diagram. The pale yellow area within the

472 dotted line depict the near-wall belt ("Near wall"). The orange dotted line showed the

473 stimulating area. The black rectangle in center shows the Aeration pump.

474 (c) The boxplot showing a comparison of the wall following time of Blind (3 species;

475 n = 9), Micro-Eyed (4 species; n = 12) and Normal-Eyed (7 species; n = 21) morphs.

476 Their handedness was also considered and the Kruskal-wallis Rank Sum Tests showed

477 that the groups spent significantly different (U = 79.49, p < 0.001) times following the

478 wall. Levels of significance indicated by ***.

479 (d-f'). Representative result of a 10-min wall-following behaviour assay for three

480 species. Vertical view of the swimming path of Blind fish (d,d'; *S. tianeensis*, B-TB),

481 Micro-Eyed fish (e,e'; *S. microphthalmus*, M-TB) and Normal-Eyed fish (f,f'; *S.*

482 *macrophthalmus*, N-TB).

483 (d, e, f) Visualization of the traces of the fish swimming paths as depicted by EthoVision.

484 (d', e', f') Heatmaps generated from the trial results of the wall-following behaviour.

485 The color bar represents the total time (min) the fish stayed in one place. Warmer colors

486 denote areas with a longer time spent, whereas cooler colors denote areas of shorter

487 time spent.

488 (g) The results of the frequency of approach in stimulation area of VAB test.

489

490   *Sinocyclocheilus* is an ancient species complex, with an estimated age for the

491   clade of nearly 10-11 Mya [9, 62].They are distributed across an enormous karstic

492   area spanning three provinces [21]. One of the main forms of speciation seems to be

493   isolation of populations over long periods, and therefore geographic speciation

494   appears to have dominated this diversification [61]. The neuromast variability seen in

495   these fishes is most likely attributable to the collective influences of both selection-

496   and drift-related evolutionary mechanisms that have played on these fishes over long

497   periods. However, the exact dynamics of the evolution of neuromasts is still an

498   intriguing question to be explored.

499

500   **Conclusion**

501   In *Sinocyclocheilus,* alongside some basic patterns, there is widespread variation in

502   cephalic neuromast patterns between species and to some extent within species. We

503   showed neuromast asymmetry with right-side enhanced for most species. For almost

504   all species, the dorsal neuromast numbers were lesser than either of the sides.

505   Furthermore, Regressed-Eyed (Blind and Micro-Eyed) species are more asymmetric

506   than the Normal-Eyed forms. Interestingly, we found the greatest degree of neuromast

507   variation and rate of evolution in Micro-Eyed species (living outside and inside caves

508   - troglophilic), this is possibly an adaptation for life in two markedly different habitats

509   types. Assays of swimming behaviour suggest a functional role of neuromasts in

510   habitat exploration. These patterns of neuromast distribution and swimming

511   behaviours are convergent with other cavefish lineages. The diversity of patterns and

512 variation can be explained by the deep evolutionary history associated with the karstic

513 region and the associated traits of this remarkable diversifications of fishes.

514

515 **Abbreviations Section:**

516 TB: Troglobitic; TP: Troglophilic; S: Surface; B: Blind; M: Micro-Eyed; N: Normal-

517 Eyed; CN: Canal neuromast; SN: Superficial neuromast; GXU: Guangxi University;

518 SL: Standard length; DEL: Delaunay Mean Distance (neuromast mean distance

519 coefficient); L: Left-Side; R: Right-Side; D: Dorsal-Side; PCC: asymmetry coefficient

520 1 = Pearson's Correlation Coefficient; OC: asymmetry coefficient 2 = Overlap-

521 Coefficient; PCA: Principal component analysis; AIC: Akaike information criterion;

522 mtDNA: Mitochondrial DNA; ND4: NADH-ubiquinone oxidoreductase chain 4; Cyt

523 b: cytochrome b gene.

524

525 **Declarations**

534   were supported also by Innovation Project of Guangxi Graduate Education

535   YCBZ2021008. These funding bodies played no role in the design of the study and

536   collection, analysis, and interpretation of data or in the writing of the manuscript.

537

538   **Conflicts of interest/Competing interests**

539   We declare no conflicts of interest.

540

541   **Ethics approval**

542   The project was approved by Guangxi Autonomous Region Government and Guangxi

543   University Ethical Clearance Committee (protocol number: GXU-2021-125).

544

545   **Consent to participate**

546   Not applicable.

547

548   **Availability of data and material**

549   All the data used in the study are provided in the electronic supplementary material.

550

551   **Authors' contributions**

552   Conceptualization – MM, BC, JBG; Fieldwork – YL, BC, TM, MM, JY;

553   Experimentation and Lab Work – BC, XL; Data Analyses – BC, TM, WD, XL;

554   Interpretation – All; Figures – BC, WD, TM; Writing original draft – BC, MM, JBG;

555   Subsequent Drafts – All; Funding acquisition – MM, JY, BC, TM, YL; Supervision –

556   MM, JBG, JY.

557

References

559   1 Jeffery WR. 2001 Cavefish as a model system in evolutionary developmental biology. *Dev. Biol*. **231**,
560   1-12. (doi:10.1006/dbio.2000.0121)

561   2 Berti R, Durand JP, Becchi S, Brizzi R, Keller N, Ruffat G. 2001 Eye degeneration in the blind cave-
562   dwelling fish *Phreatichthys andruzzii*. *Can. J. Zool*. **79**, 1278-1285. (doi:10.1139/z01-084)

563   3 Jeffery WR. 2009 Regressive evolution in *Astyanax* cavefish. *Annu. Rev. Genet*. **43**, 25-47.
564   (doi:10.1146/annurev-genet-102108-134216)

565   4 Niemiller ML, Fitzpatrick BM, Miller BT. 2008 Recent divergence with gene flow in Tennessee cave
566   salamanders (Plethodontidae: *Gyrinophilus*) inferred from gene genealogies. *Mol. Ecol*. **17**, 2258-2275.
567   (doi:10.1111/j.1365-294X.2008.03750.x)

568   5 Jeffery WR, Strickler AG, Guiney S, Heyser DG, Tomarev SI. 2000 *Prox 1* in eye degeneration and
569   sensory organ compensation during development and evolution of the cavefish *Astyanax*. *Dev. Genes*
570   *Evol*. **210**, 223-230. (doi:10.1007/s004270050308)

571   6 Wilkens H, Strecker U. 2003 Convergent evolution of the cavefish *Astyanax* (Characidae, Teleostei):
572   genetic evidence from reduced eye-size and pigmentation. *Biol. J. Linn. Soc*. **80**, 545-554.
573   (doi:10.1111/j.1095-8312.2003.00230.x)

574   7 Yoshizawa M, Jeffery WR. 2011 Evolutionary tuning of an adaptive behavior requires enhancement
575   of the neuromast sensory system. *Commun. Integr. Biol*. **4**, 89-91. (doi:10.4161/cib.14118)

576   8 Yang JXet al.. 2016 The *Sinocyclocheilus* cavefish genome provides insights into cave adaptation.
577   *BMC Biol*. **14**, 1. (doi:10.1186/s12915-015-0223-4)

578   9 Mao TR, Liu YW, Meegaskumbura M, Yang J, Ellepola G, Senevirathne G, Fu C, Gross JB, Pie MR.
579   2021 Evolution in *Sinocyclocheilus* cavefish is marked by rate shifts, reversals, and origin of novel traits.
580   *BMC Ecol. Evol*. **21**, 45. (doi:10.1186/s12862-021-01776-y)

581   10 Cahn PH. 1989 The mechanosensory lateral line: neurobiology and evolution. *BioScience*. **40**, 215-
582   216. (doi:10.2307/1311373)

583   11 Webb JF, Shirey JE. 2003 Postembryonic development of the cranial lateral line canals and
584   neuromasts in zebrafish. *Dev. Dynam*. **228**, 370-385. (doi:10.1002/dvdy.10385)

585   12 Fritzsch B, Wahnschaffe U. 1983 The electroreceptive ampullary organs of urodeles. *Cell Tissue Res*.
586   **229**, 483-503. (doi:10.1007/BF00207693)

587   13 Smith S. 1996 Pattern formation in the urodele mechanoreceptive lateral line: What features can be
588   exploited for the study of development and evolution? *Int. J. Dev. Biol*. **40**, 727-733. (doi:10.1016/0141-
589   8130(96)01109-9)

590   14 Bird NC, Webb JF. 2014 Heterochrony, modularity, and the functional evolution of the
591   mechanosensory lateral line canal system of fishes. *EvoDevo*. **5**, 21. (doi:10.1186/2041-9139-5-21)

592   15 Gross JB, Gangidine A, Powers AK. 2016 Asymmetric facial bone fragmentation mirrors asymmetric
593   distribution of cranial neuromasts in blind Mexican cavefish. *Symmetry*. **8**, 118.
594   (doi:10.3390/sym8110118)

595   16 Elipot Y, Hinaux H, Callebert J, Rétaux S. 2013 Evolutionary shift from fighting to foraging in blind
596   cavefish through changes in the serotonin network. *Curr. Biol*. **23**, 1-10. (doi:10.1016/j.cub.2012.10.044)

597   17 Yoshizawa M. 2015 Behaviors of cavefish offer insight into developmental evolution. *Mol. Reprod.*

598 *Dev*. **82**, 268-280. (doi:10.1002/mrd.22471)

599 18 Jiang Y, Peichel CL, Torrance L, Rizvi Z, Thompson S, Palivela VV, Pham H, Ling F, Bolnick DI.
600 2017 Sensory trait variation contributes to biased dispersal of threespine stickleback in flowing water. *J.*
601 *Evol. Biol*. **30**, 681-695. (doi:10.1111/jeb.13035)

602 19 Simon V, Hyacinthe C, Rétaux S. 2019 Breeding behavior in the blind Mexican cavefish and its river-
603 dwelling conspecific. *PLoS ONE*. **14**, e0212591. (doi:10.1371/journal.pone.0212591)

604 20 Ma ZQ, Herzog H, Jiang YG, Zhao YH, Zhang DY. 2020 Exquisite structure of the lateral line system
605 in eyeless cavefish *Sinocyclocheilus tianlinensis* contrast to eyed *Sinocyclocheilus macrophthalmus*
606 (Cypriniformes: Cyprinidae). *Integr. Zool*. **15**, 314-328. (doi:10.1111/1749-4877.12430)

607 21 Romero A, Zhao YH, Chen XY. 2009 The hypogean fishes of China. *Environ. Biol. Fishes*. **86**, 211-
608 278. (doi:10.1007/s10641-009-9441-3)

609 22 Zhao YH, Zhang CG. 2009 *Endemic fishes of Sinocyclocheilus (Cypriniformes: Cyprinidae) in China*
610 *-- Species diversity, cave adaptation, systematics and zoogeography*. Beijing: Science Press.

611 23 Webb JF, Northcutt RG. 1997 Morphology and distribution of pit organs and canal neuromasts in
612 non-teleost bony fishes. *Brain Behav. Evol*. **50**, 139-151. (doi:10.1159/000113328)

613 24 Powers AK, Berning DJ, Gross JB. 2020 Parallel evolution of regressive and constructive craniofacial
614 traits across distinct populations of *Astyanax mexicanus* cavefish. *J. Exp. Zool. B Mol. Dev. Evol*. **334**,
615 450-462. (doi:10.1002/jez.b.22932)

616 25 George PL, Borouchaki H. 1998 *Delaunay triangulation and meshing: application to finite elements*.
617 Paris: Hermès.

618 26 Aurenhammer F, Klein R, Lee D-T. 2012 *Voronoi diagrams and delaunay triangulations*. World
619 Scientific.

620 27 Lee DT, Schachter BJ. 1980 Two algorithms for constructing a delaunay triangulation. *Int. J. Parallel*
621 *Program*. **9**, 219-242. (doi:10.1007/BF00977785)

622 28 Palmer AR, Strobeck C, Chippindale AK. 1993 Bilateral variation and the evolutionary origin of
623 macroscopic asymmetries. *Genetica*. **89**, 201-218. (doi:10.1007/BF02424514)

624 29 Gorlewicz A, Krawczyk K, Szczepankiewicz AA, Trzaskoma P, Mulle C, Wilczynski GM. 2020
625 Colocalization colormap – an ImageJ Plugin for the quantification and visualization of colocalized
626 signals. *Neuroinformatics*. **18**, 661-664. (doi:10.1007/s12021-020-09465-9)

627 30 Zeitvogel F, Schmid G, Hao L, Ingino P, Obst M. 2016 ScatterJ: An ImageJ plugin for the evaluation
628 of analytical microscopy datasets. *J. Microsc*. **261**, 148-156. (doi:10.1111/jmi.12187)

629 31 Cordelières F, Bolte S. 2008 JACoP v2.0: improving the user experience with co-localization studies.
630 *ImageJ User & Developer Conference*. 174-181.

631 32 Wang YS, Wu QH, Hu MQ, Liu B, Chai ZY, Huang R, Wang Y, Xu HD, Zhou L, Zheng LH*, et al.*
632 2017 Ligand- and voltage-gated Ca2+ channels differentially regulate the mode of vesicular neuropeptide
633 release in mammalian sensory neurons. *Sci. Signal*. **10**, eaal1683. (doi:10.1126/scisignal.aal1683)

634 33 Bolte S, Cordelières FP. 2007 A guided tour into subcellular colocalization in light microscopy. *J.*
635 *Microsc*. **224**, 213-232. (doi:10.1111/j.1365-2818.2006.01706.x)

636 34 Dunn KW, Kamocka MM, McDonald JH. 2011 A practical guide to evaluating colocalization in
637 biological microscopy. *Am. J. Physiol. Cell Physiol*. **300**, C723-C742. (doi:10.1152/ajpcell.00462.2010)

638 35 Manders EM, Stap J, Brakenhoff GJ, van Driel R, Aten JA. 1992 Dynamics of three-dimensional
639 replication patterns during the S-phase, analysed by double labelling of DNA and confocal microscopy.
640 *J. Cell Sci*. **103**, 857-862. (doi:10.1242/jcs.103.3.857)

641 36 Zinchuk V, Grossenbacher Zinchuk O. 2009 Recent advances in quantitative colocalization analysis:

642   focus on neuroscience. *Prog. Histochem. Cytochem*. **44**, 125-172. (doi:10.1016/j.proghi.2009.03.001)

643   37 Huelsenbeck JP, Ronquist F, Nielsen R, Bollback JP. 2001 Bayesian inference of phylogeny and its

644   impact on evolutionary biology. *Science*. **294**, 2310-2314. (doi:10.1126/science.1065889)

645   38 Revell LJ. 2012 Phytools: an R package for phylogenetic comparative biology (and other things).

646   *Methods Ecol. Evol*. **3**, 217-223. (doi:10.1111/j.2041-210X.2011.00169.x)

647   39 Planidin NP, Reimchen TE. 2021 Ecological predictors of lateral line asymmetry in stickleback

648   (*Gasterosteus aculeatus*). *Evol. Ecol*. **35**, 609-629. (doi:10.1007/s10682-021-10117-w)

649   40 Sharma S, Coombs S, Patton P, de Perera TB. 2009 The function of wall-following behaviors in the

650   Mexican blind cavefish and a sighted relative, the Mexican tetra (*Astyanax*). *J. Comp. Physiol. A*. **195**,

651   225-240. (doi:10.1007/s00359-008-0400-9)

652   41 Patton P, Windsor S, Coombs S. 2010 Active wall following by Mexican blind cavefish (*Astyanax*

653   *mexicanus*). *J. Comp. Physiol. A*. **196**, 853-867. (doi:10.1007/s00359-010-0567-8)

654   42 Burt de Perera T, Braithwaite VA. 2005 Laterality in a non-visual sensory modality — the lateral line

655   of fish. *Curr. Biol*. **15**, 241-242. (doi:10.1016/j.cub.2005.03.035)

656   43 Jiang YG, Fu JC, Zhang DY, Zhao YH. 2016 Investigation on the lateral line systems of two cavefish:

657   *Sinocyclocheilus Macrophthalmus* and *S. Microphthalmus* (Cypriniformes: Cyprinidae). *J. Bionic Eng*.

658   **13**, 108-114. (doi:10.1016/S1672-6529(14)60164-5)

659   44 McGaugh SE, Weaver S, Gilbertson EN, Garrett B, Rudeen ML, Grieb S, Roberts J, Donny A,

660   Marchetto P, Gluesenkamp AG. 2020 Evidence for rapid phenotypic and behavioural shifts in a recently

661   established cavefish population. *Biol. J. Linn. Soc*. **129**, 143-161. (doi:10.1093/biolinnean/blz162)

662   45 Dezfuli BS, Magosso S, Simoni E, Hills K, Berti R. 2009 Ultrastructure and distribution of superficial

663   neuromasts of blind cavefish, *Phreatichthys andruzzii*, juveniles. *Microsc. Res. Tech*. **72**, 665-671.

664   (doi:10.1002/jemt.20714)

665   46 Powers AK, Kaplan SA, Boggs TE, Gross JB. 2018 Facial bone fragmentation in blind cavefish arises

666   through two unusual ossification processes. *Sci. Rep*. **8**, 7015. (doi:10.1038/s41598-018-25107-2)

667   47 Soares D, Niemiller ML. 2020 Variation in cephalic neuromasts surface and cave-dwelling fishes of

668   the family amblyopsidae (teleostei: percopsiformes). *J. Cave Karst Stud*. **82**, 198-209.

669   (doi:10.4311/2019LSC0115)

670   48 Trokovic N, Herczeg G, Ghani NIA, Shikano T, Merilä J. 2012 High levels of fluctuating asymmetry

671   in isolated stickleback populations. *BMC Evol. Biol*. **12**, 115. (doi:10.1186/1471-2148-12-115)

672   49 Soares D, Niemiller ML. 2020 Extreme Adaptation in Caves. *Anat. Rec*. **303**, 15-23.

673   (doi:10.1002/ar.24044)

674   50 Krishnan J, Rohner N. 2017 Cavefish and the basis for eye loss. *Philos. Trans. R. Soc. Lond., B. Biol.*

675   *Sci*. **372**, 20150487. (doi:10.1098/rstb.2015.0487)

676   51 Fernandes VFL, Macaspac C, Lu L, Yoshizawa M. 2018 Evolution of the developmental plasticity

677   and a coupling between left mechanosensory neuromasts and an adaptive foraging behavior. *Dev. Biol*.

678   **441**, 262-271. (doi:10.1016/j.ydbio.2018.05.012)

679   52 Coombs S, Janssen J, Webb JF. Year Diversity of lateral line systems: evolutionary and functional

680   considerations. In: J. Atema, R. R. Fay, A. N. Popper, W. N. Tavolga, editors. Sensory Biology of Aquatic

681   Animals; 1988; New York, NY: Springer New York; 1988. 553-593.

682   53 Montgomery JC, Coombs S, Baker CF. 2001 The mechanosensory lateral line system of the hypogean

683   form of *Astyanax Fasciatus*. *Environ. Biol. Fishes*. **62**, 87-96. (doi:10.1023/A:1011873111454)

684   54 Yamamoto Y, Byerly MS, Jackman WR, Jeffery WR. 2009 Pleiotropic functions of embryonic *sonic*

685   *hedgehog* expression link jaw and taste bud amplification with eye loss during cavefish evolution. *Dev.*

686 *Biol*. **330**, 200-211. (doi:10.1016/j.ydbio.2009.03.003)

687 55 Zhao YH, Zhang CG. 2006 Past research and future development on endemic Chinese cavefish of

688 the genus *Sinocyclocheilus* (Cypriniformes, Cyprinidae). *Acta Zootaxonomica Sinica*. **31**, 769-777.

689 56 He Y, Chen XY, Xiao TQ, Yang JX. 2013 Three-dimensional morphology of the *Sinocyclocheilus*

690 *hyalinus* (Cypriniformes : Cyprinidae) horn based on synchrotron X-ray microtomography. *Zool. Res*.

691 **34**, 128-134. (doi:10.11813/j.issn.0254-5853.2013.E4-5.E128)

692 57 Teyke T. 1990 Morphological differences in neuromasts of the blind cave fish *Astyanax hubbsi* and

693 the sighted river fish *Astyanax mexicanus*. *Brain Behav. Evol*. **35**, 23-30. (doi:10.1159/000115853)

694 58 Wark AR, Peichel CL. 2010 Lateral line diversity among ecologically divergent threespine

695 stickleback populations. *J. Exp. Biol*. **213**, 108-117. (doi:10.1242/jeb.031625)

696 59 Zhao YH, Watanabe K, Zhang CG. 2006 *Sinocyclocheilus donglanensis*, a new cavefish (Teleostei:

697 Cypriniformes) from Guangxi, China. *Ichthyol. Res*. **53**, 121-128. (doi:10.1007/s10228-005-0317-z)

698 60 Culver D, Pipan T. 2019 *The biology of caves and other subterranean habitats*.

699 61 Xiao H, Chen SY, Liu ZM, Zhang RD, Li WX, Zan RG, Zhang YP. 2005 Molecular phylogeny of

700 *Sinocyclocheilus* (Cypriniformes: Cyprinidae) inferred from mitochondrial DNA sequences. *Mol.*

701 *Phylogenet. Evol*. **36**, 67-77. (doi:10.1016/j.ympev.2004.12.007)

702 62 Li ZQ, Guo BC, Li JB, He SP, Chen YY. 2008 Bayesian mixed models and divergence time estimation

703 of Chinese cavefishes (Cyprinidae: *Sinocyclocheilus*). *Chinese Science Bulletin*. **53**, 2342-2352.

704 (doi:10.1007/s11434-008-0297-2)

705